CHEMISTRY

Catalytic photooxygenation degrades brain Aβ in vivo

Nozomu Nagashima, Shuta Ozawa, Masahiro Furuta, Miku Oi, Yukiko Hori*, Taisuke Tomita*, Youhei Sohma*, Motomu Kanai*

Protein degradation induced by small molecules by recruiting endogenous protein degradation systems, such as ubiquitin-proteasome systems, to disease-related proteins is an emerging concept to inhibit the function of undruggable proteins. Protein targets without reliable ligands and/or existing outside the cells where ubiquitin-proteasome systems do not exist, however, are beyond the scope of currently available protein degradation strategies. Here, we disclose photooxygenation catalyst 7 that permeates the blood-brain barrier and selectively and directly degrades an extracellular Alzheimer's disease–related undruggable protein, amyloid-β protein (Aβ). Key was the identification of a compact but orange color visible light–activatable chemical catalyst whose activity can be switched on/off according to its molecular mobility, thereby ensuring high selectivity for aggregated Aβ. Chemical catalyst–promoted protein degradation can be applied universally for attenuating extracellular amyloids and various pathogenic proteins and is thus a new entry to induced protein degradation strategies.

INTRODUCTION

A general mode of action for traditional drug molecules is to bind target proteins and inhibit their functions. The functions of some proteins, however, are difficult to inhibit using binder molecules. Those proteins are considered "undruggable" targets. An emerging concept for inhibiting the function of undruggable proteins is drug-induced degradation using endogenous protein degradation mechanisms (*1*, *2*). PROTACs (proteolysis targeting chimeras), a typical example of this strategy, are bifunctional molecules in which a ligand (binder) for a target protein and a ligand for E3 ligase are covalently tethered. PROTACs promote the degradation of target proteins by recruiting the proteasome system to the target proteins via ubiquitination. Moreover, PROTACs can act catalytically due to the turnover of the ligand binding. The scope of PROTACs, however, is limited to proteins present inside the cells, where the ubiquitin-proteasome system exists. In addition, as required for traditional drugs, the fidelity of the target selectivity depends on the selectivity of the ligand moiety. These features imply that protein targets without reliable ligands or that exist outside of cells are beyond the scope of the currently available protein degradation strategies, especially in vivo. Here, we disclose a chemical catalyst that selectively and directly degrades and attenuates an extracellular undruggable protein, amyloid-β protein (Aβ), by promoting photooxygenation reactions in an Alzheimer's disease (AD) model mouse brain.

Amyloidosis is a class of diseases whose etiology is intimately related to the deposition of aberrant protein aggregates, amyloid oligomers and fibrils, inside and outside of cells (*3*, *4*). Amyloids contain a characteristic quaternary structure called a cross–β-sheet. Many amyloidosis-related diseases are considered intractable today. In particular, AD, an amyloidosis-related brain disease, is an age-related neurodegenerative disorder that causes a progressive loss of memory. The number of patients with AD in the world is enormous and continues to increase, having great negative social impact worldwide. The initiation step of the neurodegenerative cascade in AD is the amyloid formation of Aβ (ca. 40 residues long). Potent inhibition of amyloid formation is difficult to achieve, however, because Aβ aggregation proceeds through protein-protein interactions across a large surface area. Some antibodies furnishing opsonization of Aβ aggregation have been developed (*5*, *6*). The low blood-brain barrier (BBB) permeability of antibodies (<0.1%) due to their gigantic molecular weight (*7*), however, may limit their efficacy. Furthermore, because Aβ aggregation is initiated more than 20 years before the onset of AD symptoms and signs, the administration of high-cost antibodies for such a long period is difficult from a medical economic viewpoint. A new therapeutic strategy for inhibiting Aβ aggregation is therefore in high demand.

Amyloid formation can be persistently inhibited by introducing irreversible chemical modifications of amyloidogenic proteins and changing their chemical and physical properties (*8*–*15*). We previously reported that aerobic oxygenation mediated by small-molecule photooxygenation catalyst **1** attenuates the aggregation and toxicity of Aβ (Fig. 1A) (*16*). The side chains of the His and Met residues of Aβ are the oxygenation sites. Because protein aggregation generally arises from hydrophobic effects, covalent installation of hydrophilic oxygen atoms to Aβ and stabilization of the hydrated states account for the photooxygenation-induced decrease in the aggregative properties of Aβ. The catalytic activity of **1** is on/off switchable by binding/nonbinding to the cross–β-sheet structure of amyloids, enabling selective oxygenation of aggregated Aβ (and other amyloids) over off-target biomacromolecules. The mechanism for the amyloid selectivity is as follows: (i) Rotation of the axial bond between electron-donor (julolidine) and acceptor (benzothiazole) moieties of **1** is hindered by binding to the cross–β-sheet of amyloids; (ii) the excited singlet state of **1**, generated by photoirradiation, transits to the triplet state through intersystem crossing only when **1** binds to amyloids, which is facilitated by the heavy atom effect of the bromine atom (*17*); and (iii) singlet oxygen ($^1O_2$) is produced only at the proximate regions of amyloids through energy transfer from the triplet state **1** to ground-state molecular oxygen ($^3O_2$). We further identified photooxygenation catalysts **2** and **3** containing the same on/off switching mechanism but absorbing tissue-permeable and less toxic longer wavelength light for excitation (>650 nm) (*18*, *19*). These catalysts can only be administered directly to inside the brains of living mice by partially disrupting the skull and brain tissue,

Graduate School of Pharmaceutical Sciences, The University of Tokyo, 7-3-1 Hongo, Bunkyo-ku, Tokyo 113-0033, Japan.
*Corresponding author. Email: yukiko-hori@mol.f.u-tokyo.ac.jp (Y.H.); taisuke@mol.f.u-tokyo.ac.jp (T.T.); ysohma@mol.f.u-tokyo.ac.jp (Y.S.); kanai@mol.f.u-tokyo.ac.jp (M.K.)

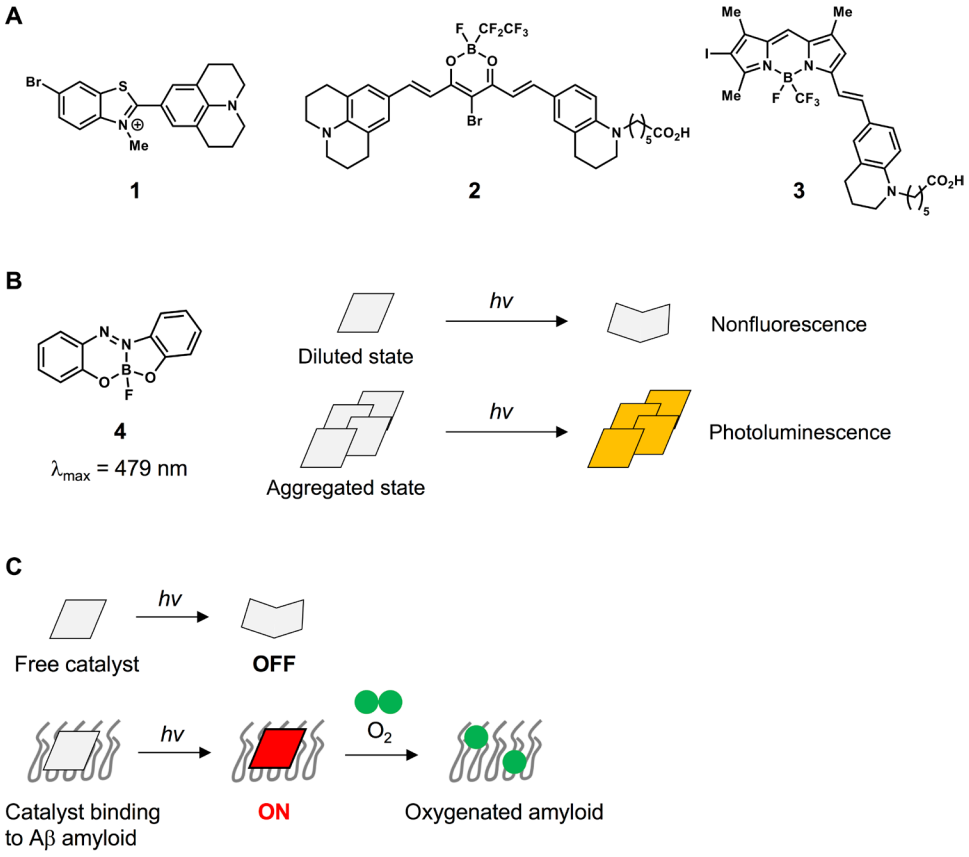

Fig. 1. Catalyst design for less invasive photooxygenation of Aβ in the brain. (**A**) Photooxygenation catalysts for Aβ previously reported by our group. (**B**) AIE properties of azobenzene-boron complex (*22*). λ_{max} values were measured in toluene. (**C**) Strategy of new photooxygenation catalyst (this work).

however, due to their negligible BBB permeability attributable to the large molecular weights (over 650) (*20*, *21*). In addition, the carboxylic acid functionality required for solubilizing the catalysts to aqueous media due to the high hydrophobicity of the photocatalytic core structures of **2** and **3** may also be disadvantageous for BBB penetration. Thus, the molecular design used in **2** and **3** to achieve long-wavelength light activation and on/off switching, i.e., a long π-conjugation system connected by an axial bond, is not compatible with BBB permeability and thus requires invasive application for use in living animals.

Given this background, in the present study, we developed a new photooxygenation catalyst with a compact chemical structure that crosses the BBB in mice when administered peripherally and can be activated with orange color visible light to induce protein degradation.

RESULTS AND DISCUSSION

Design and optimization of a new photooxygenation catalyst

As a new scaffold for photooxygenation catalysts fulfilling the above requirements, we were inspired by the structure and properties of fused azobenzene-boron complex **4**, reported as a photoluminescent molecule by Tanaka and Chujo's group (Fig. 1B) (*22*). Compound **4** has a small molecular weight of 242 but has a relatively long maximum absorption wavelength of 479 nm. Density functional theory (DFT) calculations indicated that the most stable structure of **4** in the ground state is near-planar [dihedral angle $\varphi_{(C-N=N-C)}$ = 165°], while the most stable structure in the excited state is considerably bent [$\varphi_{(C-N=N-C)}$ = 141°]. Thus, excited **4** generated by light irradiation in a diluted solution likely relaxes to the ground state by the molecular motion from a planar to bent structure, resulting in nonfluorescence. When the molecular motion is suppressed by stacking in the aggregated state, however, excited **4** decays through fluorescence emission. We envisioned that the aggregation-induced emission (AIE) property of **4** (*23*) could be an alternative switch mechanism for selective photooxygenation catalysts (Fig. 1C). Thus, in the absence of Aβ amyloid, the excited catalyst relaxes through molecular motion, furnishing no oxygenation activity. In the presence of Aβ amyloid, however, the molecular motion of the catalyst is hindered by binding to the amyloid, analogous to the aggregation state of **4**, facilitating the relaxation pathway through intersystem crossing to produce $^1O_2$. As a stilbene skeleton, a structural analog of azobenzene, is a known motif of binding molecules for aggregated Aβ (*24*), we anticipated that azobenzene-boron complexes would bind to aggregated Aβ. Therefore, we designed **5** as a selective photooxygenation catalyst of Aβ amyloid.

We first examined the absorption spectrum and solubility of **5** (*22*) with two bromine atoms (Fig. 2A and fig. S1A). The maximum absorption wavelength of **5** was 487 nm, and its solubility in biocompatible solvents [H_2O, dimethyl sulfoxide (DMSO), ethanol (EtOH), etc.] was consistently small. The low solubility of **5** in polar solvents was likely due to the planar structure of the molecule, inducing

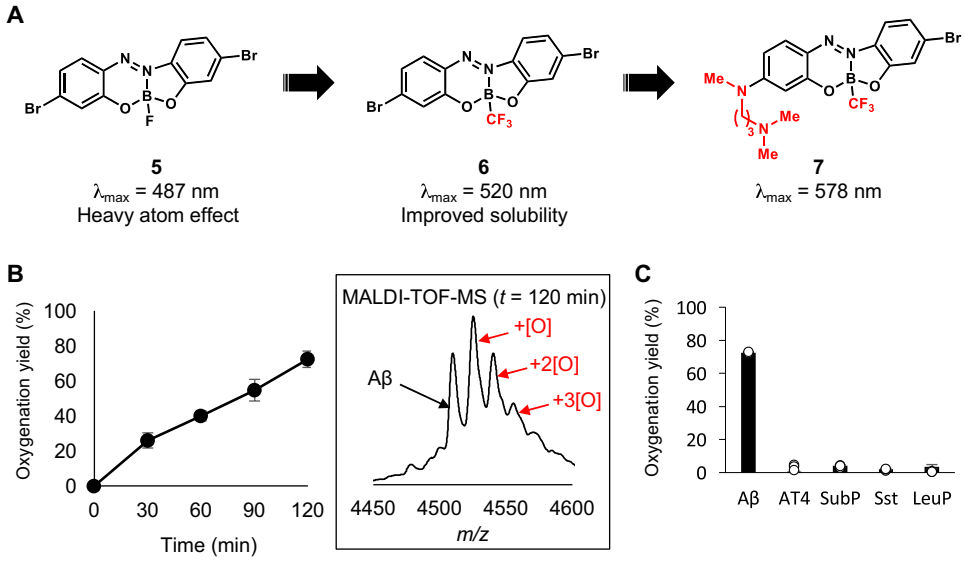

Fig. 2. Structure optimization and properties of photooxygenation catalysts. (**A**) Molecular design of photooxygenation catalyst **7** for Aβ. λ_{max} was measured in $CHCl_3$. (**B**) Photooxygenation of aggregated Aβ using **7**. A phosphate buffer solution (pH 7.4) containing $A\beta_{1-42}$ (20 μM) and **7** (40 μM) was photoirradiated ($\lambda = 595$ nm) at 37°C for certain time periods, and the reaction progress was analyzed using MALDI-TOF-MS ($n = 3$, mean ± SD). Inset: MALDI-TOF-MS chart at 120 min. The oxygenation yield of $A\beta_{1-42}$ under light irradiation for 120 min without **7** was below 5%. (**C**) Aβ selectivity of the photooxygenation with **7**. A phosphate buffer solution (pH 7.4) containing aggregated Aβ, angiotensin-IV (AT4; amino acid sequence with underlined potential oxidation site: VYIHPF), [Tyr^8]–substance P (SubP; RPKPQQFYGLM-NH_2), somatostatin (Sst; AGCKNFFWKTFTSC), or leuprorelin (LeuP; PyroEHWSYLLRP) (20 μM each) was photoirradiated in the presence of **7** (40 μM) at 595 nm (10 mW) at 37°C for 120 min, and each reaction mixture was analyzed by MALDI-TOF-MS ($n = 3$, mean ± SD).

self-association. Therefore, we introduced a bulky CF_3 group at the boron center to prevent self-association and designed compound **6**. The solubility of **6** in polar solvents was markedly improved. Moreover, the maximum absorption wavelength of **6** was red-shifted to 520 nm due to the stronger electron-withdrawing effects of the CF_3 group on the boron center than the F atom in **5**. We next introduced an amino group to a benzene ring as an electron donor (compound **7**). As a result, **7** absorbed orange color visible light with a maximum absorption wavelength of 578 nm (fig. S1A). The absorption intensity of **7** in phosphate buffer was also improved because of high water solubility over 100 μM (fig. S1B).

Selective photooxygenation of Aβ amyloid using 7

To investigate the photooxygenation potency of **7**, a phosphate buffer solution (pH 7.4) containing aggregated $A\beta_{1-42}$ (20 μM, amino acid sequence: DAEFRHDSGYEVHHQKLVFFAEDVGSNKGAIIGLMVGGVVIA) and **7** (40 μM) was irradiated using a 595-nm light-emitting diode (LED) at 37°C, and the reaction was monitored by matrix-assisted laser desorption ionization time-of-flight mass spectrometry (MALDI-TOF-MS) at certain time points (Fig. 2B). The oxygen atom adducts of Aβ (n[O], n = 1 to 3) increased according to the reaction time, with the yield reaching 73% at 2 hours. Liquid chromatography with tandem MS (LC-MS/MS) analysis after enzymatic digestion of the oxygenated Aβ revealed that the oxygen atoms were introduced at the His^6, His^{13}, His^{14}, and Met^{35} residues of Aβ (fig. S2). We assessed the Aβ selectivity of oxygenation with **7** using angiotensin-IV (VYIHPF), [Tyr^8]–substance P (RPKPQQFYGLM-NH_2), somatostatin (AGCKNFFWKTFTSC), and leuprorelin (PyroEHWSYLLRP) as off-target substrates (Fig. 2C). The oxygenation yields of the off-target peptides were all less than 4% under conditions in which Aβ was oxygenated at 73% yield. In addition, **7** showed significant catalytic activity to homogeneous $A\beta_{1-42}$ oligomer samples (*18*), with the oxygenation yield of 27% under photoirradiation for 30 min. The oxygenation activity of **7** was, however, considerably diminished for a less aggregative $A\beta_{1-42}$ analog that existed mainly as a monomer state (fig. S3). These results indicate that the on/off switching function of the catalytic activity of **7** depending on binding/nonbinding to the amyloid substrates facilitated aggregated Aβ-selective oxygenation (see below for the mechanistic study).

Mechanistic insights into the on/off switch of catalyst 7

We measured the absorbance and fluorescence spectra of **7** in the absence and presence of aggregated Aβ. The maximum absorbance of **7** red-shifted from 578 to 588 nm in the presence of aggregated Aβ, suggesting that **7** interacted with aggregated Aβ and underwent conformational change (fig. S4). In addition, the fluorescence intensity of **7** was markedly higher in the presence of aggregated Aβ than in the absence of Aβ (Fig. 3A). These results support our hypothesis that the binding of **7** with aggregated Aβ interferes with its no emission relaxation pathway by molecular motion, similar to the AIE mechanism of **4**, thereby extending the lifetime of the excited state. A quartz crystal microbalance study revealed that the K_d (dissociation constant) value of **7** with aggregated Aβ was 3.4 μM, thus indicating an affinity similar to that of our previous catalysts (*18*).

The production of $^1O_2$ using **7** was validated by the consumption of furfuryl alcohol, which specifically reacts with $^1O_2$ (Fig. 3B) (*25*). The amount of furfuryl alcohol decreased by ca. 10% at 180 min and ca. 27% at 240 min in the presence of aggregated Aβ and light irradiation, while the amount of furfuryl alcohol remained unchanged without Aβ but with light irradiation, suggesting that $^1O_2$ is generated via binding of **7** with aggregated Aβ. The bromine atom in **7** was essential for the high catalyst activity; substitution of the bromine atom with a hydrogen atom (compound **8**; Fig. 3C) and a chlorine atom (fig. S5) markedly weakened the oxygenation activity.

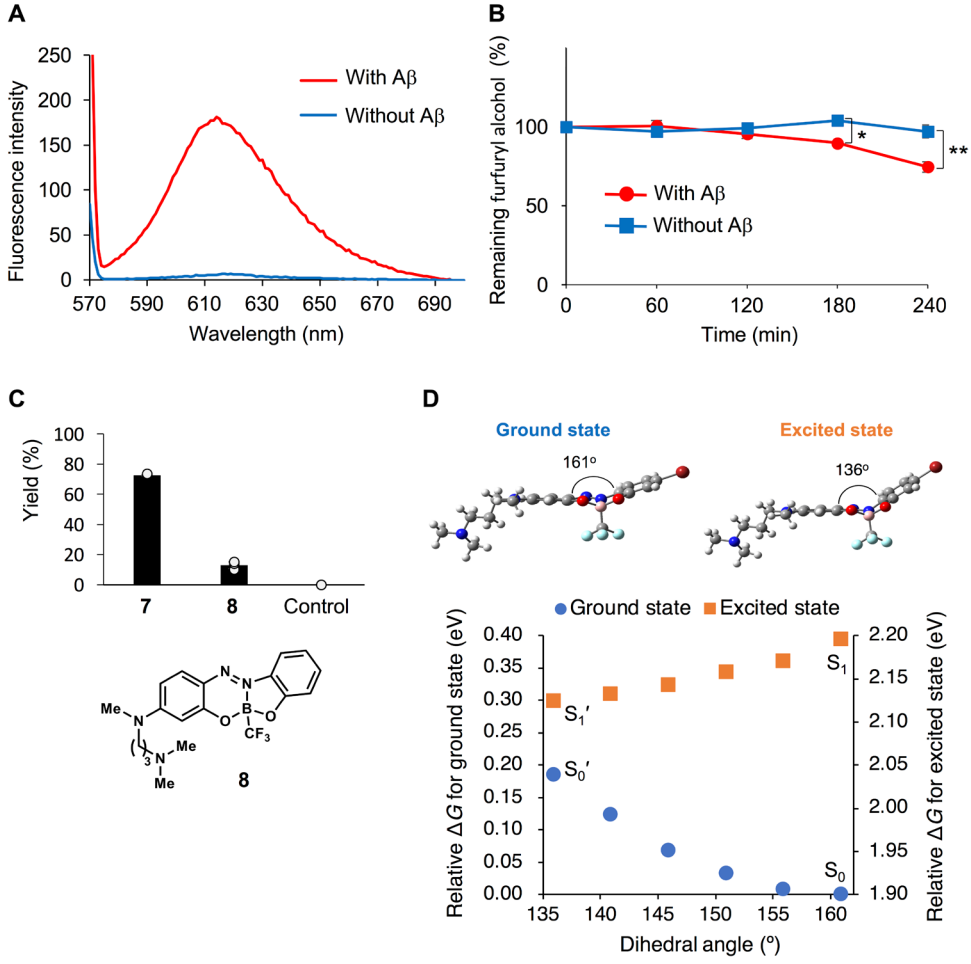

Fig. 3. Mechanistic insight into Aβ-selective photooxygenation with 7. (**A**) Fluorescence spectra of **7** with or without aggregated Aβ. A phosphate buffer solution (pH 7.4) containing **7** (20 μM) with or without $Aβ_{1–42}$ (20 μM) was incubated at 37°C for 1 hour. **7** was excited at λ = 560 nm. (**B**) Assessment of $^1O_2$ production. A phosphate buffer solution (pH 7.4) containing **7** (200 μM) and furfuryl alcohol (FurA; 2 mM) with or without aggregated $Aβ_{1–42}$ (20 μM) was photoirradiated (λ = 595 nm) at 37°C for certain time periods, and the remaining FurA was quantified by ultraviolet (UV) absorbance ($n = 3$, mean ± SD, $^*P < 0.05$, $^{**}P < 0.01$ by t test). (**C**) Effects of the bromine atom in the catalyst on the photooxygenation activity. A phosphate buffer solution (pH 7.4) containing Aβ (20 μM) and **7**, **8**, or none (for control) (40 μM) was photoirradiated (λ = 595 nm) at 37°C for 2 hours. Yield of oxygenated Aβ was analyzed by MALDI-TOF-MS ($n = 3$, mean ± SD). (**D**) Top: Optimized structures in the ground and excited states of **7** calculated by DFT and TD-DFT, respectively. Bottom: Relationships between ΔG and dihedral angles (°) of the two phenyl groups ($136° < \varphi_{(C–N=N–C)} < 161°$) in **7** at the ground and excited states, calculated by DFT and TD-DFT, respectively. ΔG is expressed relative to the minimum energy at the ground state.

The switching mechanism of **7** in the absence or presence of aggregated Aβ was investigated from theoretical calculations. Gibbs free energies of **7** with various dihedral angles of the two phenyl groups [$\varphi_{(C–N=N–C)}$] were calculated for the ground state and excited state by DFT and time-dependent (TD)–DFT, respectively. The lowest-energy conformation in the ground state was near-planar ($\varphi_{(C–N=N–C)} = 161°$), while the optimized conformation in the excited state via a Franck-Condon structure was the bent structure ($\varphi_{(C–N=N–C)} = 136°$) (Fig. 3D, upper part). The relaxed potential energy surface scan revealed that the potential energy gradually decayed depending on the dihedral angle between 136° and 161° (i.e., $S_1 \rightarrow S_1'$ in the excited state and $S_0' \rightarrow S_0$ in the ground state) (Fig. 3D, lower part). Therefore, in the absence of aggregated Aβ when the molecule is freely mobile, emission annihilation proceeded during the relaxation from planar (S_1) to bent structure (S_1'). In the presence of aggregated Aβ, however, the molecular motion of **7** from S_1 to S_1' should be hindered by binding. Because the energy gap between S_1 and S_0 and the lifetime of S_1 were both relatively great, S_1 decayed through intersystem crossing followed by energy transfer to $^3O_2$, generating $^1O_2$ as the active species for oxygenation. Therefore, the theoretical calculation supports the idea that the molecular motion is the on/off switch of the oxygenation activity of **7** (fig. S6).

The reactivity of **7** to other aggregated amyloid proteins, i.e., amylin, α-synuclein, and insulin, was also examined (fig. S7). All three substrates were oxygenated in high yield. As a control, a nonaggregated physiologic form of insulin did not undergo oxygenation in the presence of **7**. These findings indicate that **7** is activated by binding to the cross–β-sheet, a general quaternary structure of amyloids.

Effects of photooxygenation on the aggregation of Aβ

The effects of photooxygenation using **7** on the aggregation of Aβ were examined using thioflavin-T (ThT), whose fluorescence intensity correlates with the cross–β-sheet structure amount (*26*). The fluorescence intensity of ThT was reduced by oxygenation of Aβ in the

presence of **7**, as compared with using only light or catalyst (Fig. 4A). Furthermore, oxygenation by **7** reduced the seeding ability of Aβ (Fig. 4B). Thus, aggregation of $Aβ_{1–40}$ was significantly slower when oxygenated $Aβ_{1–42}$ was seeded than when nonoxygenated native $Aβ_{1–42}$ was seeded ($Aβ_{1–40}$:seed = 99:1 in both cases) [note that aggregation of $Aβ_{1–42}$ is too fast for seeding experiments, and it is, therefore, a common method to use less aggregative $Aβ_{1–40}$ than $Aβ_{1–42}$ for evaluation of the seeding ability (*27*)]. The seeding properties that are attenuated by the catalytic photooxygenation must be critical for inhibiting Aβ aggregation in vitro (Fig. 4A) and in vivo (see the next section). The toxicity of oxygenated Aβ to rat cortical primary neurons was lower than that of native Aβ (Fig. 4C). Thus, the viability of neuronal cells treated with oxygenated Aβ by **7** under photoirradiation (lane 8) was significantly higher than that treated with native Aβ (lane 5), Aβ + photoirradiation without **7** (lane 6), or Aβ + **7** without photoirradiation (lane 7). The lower toxicity of oxygenated Aβ was also observed when using rat pheochromocytoma PC12 cells (fig. S8).

Photooxygenation of Aβ in the mouse brain

The BBB permeability of **7** was evaluated to determine whether **7** could oxygenate Aβ in the mouse brain by its peripheral administration instead of the previous intraventricular administration accompanied by invasive surgery (Fig. 5A). Mice (8 weeks old, C57BL/6J) were intravenously injected with **7** through the eye socket, and the amount of **7** in the brain was analyzed by high-performance liquid chromatography (HPLC). Catalyst **7** was recovered in 0.58, 1.48, and 1.05% yield at 10 min, 60 min, and 1 day after the administration, respectively. The BBB permeability of **7** was considerably higher than that of previously reported catalysts **2** (<0.02%) and **3** (0.029 to 0.032%) and comparable to that of practical Aβ probes (*28*).

We then carried out the catalytic photooxygenation of Aβ using **7** in brain lysate (Fig. 5B). Brain lysate was prepared from a 7-month-old *App* knock-in mouse expressing human Aβ with the Arctic mutation (E22G) ($App^{NL\text{-}G\text{-}F/NL\text{-}G\text{-}F}$) (*29*). Western blotting analysis with an anti-Aβ antibody showed that 10-kDa Aβ derivatives were generated only in the photooxygenation sample (**7** + Light), and the band density increased in a TD manner. This 10-kDa band should be a dimerized product derived from two Aβ molecules via the oxygenation of a His residue. Oxidative dimerization (and oligomerization) of peptides through cross-linking between oxidized His and nucleophilic amino acid residues such as Lys or His was previously reported (Fig. 5C) (*30*–*33*). Accordingly, catalyst **7** photooxygenated Aβ present in low concentrations in brain lysate containing a large number of off-target molecules. Many soluble proteins in the lysate remained intact under photooxygenation using **7**, while they were degraded by photooxygenation with riboflavin, a catalyst without the on/off switching function (fig. S9) (*12*). The selectivity of **7** to Aβ over other molecules was also supported by fluorescent staining

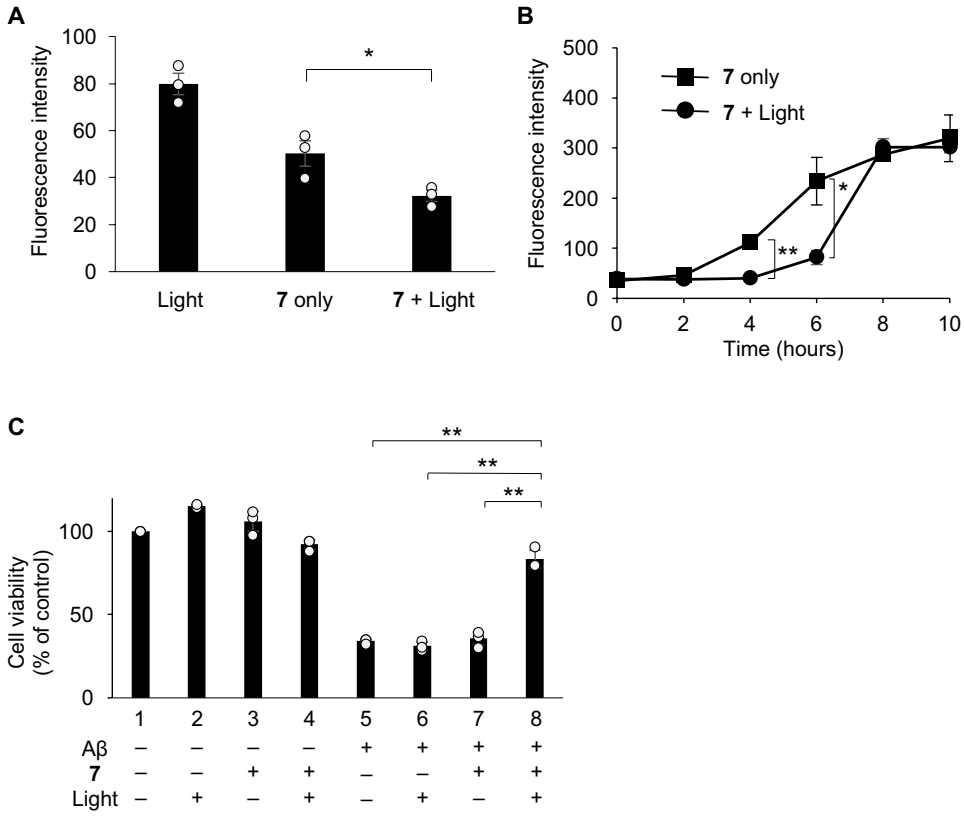

Fig. 4. Effects of 7-mediated photooxygenation on propensities of Aβ. (**A**) A phosphate buffer solution (pH 7.4) containing $Aβ_{1–42}$ (20 μM) and **7** (2 μM) was photoirradiated (λ = 595 nm) at 37°C for 18 hours. The reaction solution was subjected to a ThT fluorescence assay ($n = 3$, mean ± SEM, $^*P < 0.05$ by *t* test). (**B**) The preformed seeds (1 mol % ratio) of $Aβ_{1–42}$ with or without photooxygenation using **7** (**7** + Light and **7** only, respectively) were added to the monomer form of $Aβ_{1–40}$ (50 μM) in phosphate buffer solution (pH 7.4), and the solution was incubated at 37°C for certain time periods. The extent of aggregation was verified by a ThT fluorescence assay ($n = 3$, mean ± SEM; $^*P < 0.05$ and $^{**}P < 0.01$ by *t* test). (**C**) A PBS solution containing aggregated Aβ (0 or 20 μM) and **7** (0 or 20 μM) was irradiated with light (λ = 595 nm) for 1 hour at 37°C. The oxygenated or nonoxygenated Aβ was added to primary neuron cell–seeded wells (final concentrations of Aβ and **7** were both 5 μM) and applied to a cell viability assay ($n = 3$, mean ± SD, $^{**}P < 0.01$ by *t* test).

A

Catalyst	Time after administration		
	10 min	60 min	1 day
2	ND	ND	–
3	0.032 ± 0.007%	0.029 ± 0.012%	ND
7	0.58 ± 0.11%	1.48 ± 0.15%	1.05 ± 0.20%

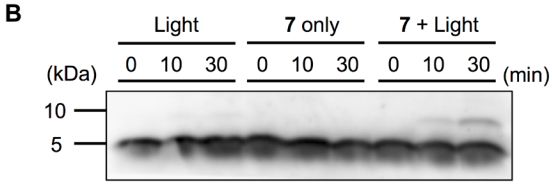

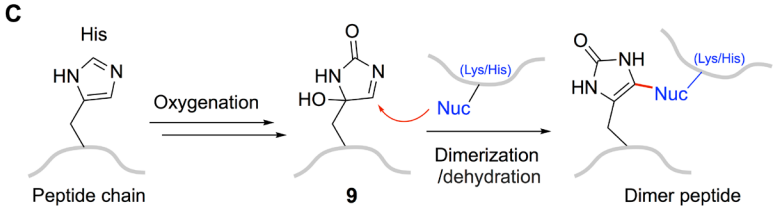

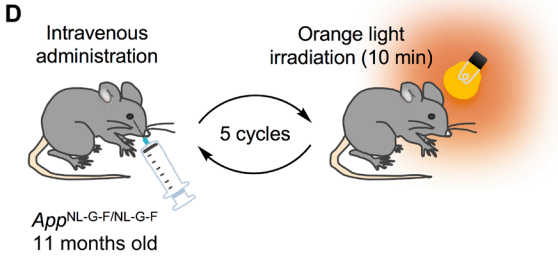

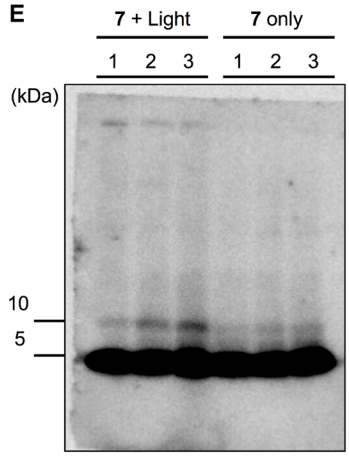

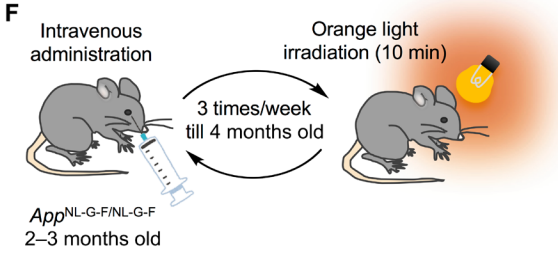

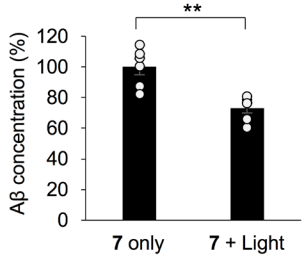

Fig. 5. Photooxygenation of Aβ in vivo. (**A**) BBB permeability of the catalysts. A solution containing catalyst was intravenously injected into the mouse ($n = 3$, mean ± SD). ND, not detected. (**B**) Photooxygenation of Aβ in the mouse brain lysate. A mixture of **7** and the brain lysate was photoirradiated for 0, 10, or 30 min and was analyzed by Western blotting. (**C**) Oxidative dimerization of peptides through cross-linking between oxidized His (**9**) and nucleophilic amino acid residues. (**D**) Aβ photooxygenation by **7** in the brain of a living mouse. A solution of **7** was intravenously injected into a mouse. After 60 min, the head was irradiated with 600-nm LED for 10 min. The operation set was repeated for five times over 5 days. (**E**) The FA fraction obtained in (D) was analyzed by Western blotting ($n = 3$). (**F**) Aβ concentration in the brain after oxygenation. A solution of **7** was intravenously injected into mice. After 60 min, the head was irradiated with 600-nm LED for 10 min. The operation set was repeated three times per week until the mice were 4 months old. Aβ concentration in the FA fraction was determined by Western blotting ($n = 6$, mean ± SEM, $^{**}P < 0.01$ by t test). The Aβ concentration (%) in **7** + Light is expressed as (Aβ band density in **7** + Light group of mice)/(Aβ band density in **7** only group of mice) × 100.

of brain sections of an *App* knock-in mouse with **7** (fig. S10). Thus, the fluorescence of **7** overlapped well with the fluorescence of thioflavin-S (ThS), a dye commonly used for staining Aβ plaques.

On the basis of these results, we examined whether Aβ in the brain of an AD model mouse could be oxygenated by administering the catalyst peripherally and irradiating light from outside the body. Thus, **7** was injected into an 11-month-old *App* knock-in mouse through the eye socket, and the head of the mouse was irradiated with 600-nm light for 10 min (Fig. 5D) [there was no obvious background toxicity under photoirradiation conditions in the presence of **7** (fig. S11)]. After repeating the operation set (administration of **7** and light irradiation) five times, Aβ in the hippocampus was analyzed by Western blotting (Fig. 5E). The amount of 10-kDa Aβ derivative was significantly increased compared with that in the control group in which **7** was administered, but photoirradiation was not conducted. Therefore, the photooxygenation reaction of Aβ proceeded in the brain of a living mouse using a therapeutically relevant less invasive method than previous report (*18*). Then, we examined the effects of the catalytic photooxygenation on the concentration of aggregated Aβ in the brain by chronic administration and photoirradiation over the skull. *App* knock-in mice start to develop Aβ plaque pathology from 2 months. Thus, the operation set (administration of **7** and light irradiation) was applied to 2- to 3-month-old *App* knock-in mice three times a week until they were 4 months old. After the final operation set, we took the hippocampus and analyzed the amount of aggregated Aβ obtained as the formic acid (FA) fraction (Fig. 5F and fig. S12). As a result, aggregated Aβ in the mouse brain treated with **7** + Light was reduced by 27% compared with the control group in which **7** was administered, but photoirradiation was not conducted. This is the first showcase demonstrating that a chemical reaction promoted by an artificial catalyst reduced the pathogenic Aβ concentration in the living mouse brain without invasive surgery (disrupting the skull and brain tissue).

In summary, we developed photooxygenation catalyst **7** based on the structure of azobenzene-boron complex exhibiting AIE. Catalyst **7** has three main characteristics required for in vivo application: (i) activation by tissue-permeable long-wavelength light irradiation, (ii) Aβ selectivity of the oxygenation reaction, and (iii) BBB permeability. These properties of **7** made it possible to oxygenate Aβ in living mouse brains using a less invasive method than previously reported that involves administration of the catalyst to the periphery and light irradiation from outside the body. Key to this success was the identification of a compact but orange color visible light–activatable chemical catalyst whose activity can be switched on/off depending on binding/nonbinding to aggregated Aβ, which controls its molecular mobility. Long-term (1 to 1.5 months) treatment using this less invasive photooxygenation method with **7** reduced the aggregated Aβ level in the mouse brain. This is an important step forward in the development of a catalytic photooxygenation strategy for clinical application. Moreover, this concept may be universally applied for degrading and attenuating other extracellular amyloids and various pathogenic proteins.

MATERIALS AND METHODS

Synthesis of 6

CF_3BF_3K (57 mg, 0.32 mmol), trimethylsilyl trifluoromethanesulfonate (97.2 μl, 0.53 mmol), and *N*,*N*-diisopropylethylamine (68.8 μl, 0.40 mmol) were added to a stirred solution of (*E*)-6,6′-(diazene-1,2-diyl)bis(3-bromophenol) (30 mg, 0.081 mmol) in tetrahydrofuran (3.0 ml), and the mixture was stirred at 60°C overnight. After cooling, the reaction mixture was concentrated in vacuo. The resulting residue was dissolved in a mixture of CH_2Cl_2 and H_2O. The water layer was extracted three times with CH_2Cl_2. The combined organic layers were washed with brine, dried over Na_2SO_4, and concentrated in vacuo. The residue was purified by column chromatography on silica gel (eluent: hexane/CH_2Cl_2 = 3:1) to afford **6** as a red solid (16.8 mg, 0.037 mmol, y. 46%). ^{1}H nuclear magnetic resonance (NMR) ($CDCl_3$, 500 MHz): δ = 7.70 (d, *J* = 4.5 Hz, 1H), 7.66 (d, *J* = 8.6 Hz, 1H), 7.42 (m, 2H), 7.33 (m, 1H), 7.26 (m, 1H); ^{13}C NMR ($CDCl_3$, 126 MHz): δ = 162.1, 144.8, 139.3, 134.5, 132.7, 132.5, 132.4, 126.7, 126.3, 123.2, 119.9, 117.7; ^{11}B NMR ($CDCl_3$, 126 MHz): δ = 0.30; ^{19}F NMR ($CDCl_3$, 369 MHz): δ = −73.6. High resolution mass spectrometry (HRMS) [atmospheric pressure chemical ionization (APCI)] mass/charge ratio (*m*/*z*) calcd for $C_{13}H_7BBr_2F_3N_2O_2^+$ $[M + H]^+$: 448.8914. Found: 448.8898.

Synthesis of 7

N,*N*,*N*′-Trimethyl-1,3-propanediamine (5.6 μl, 0.038 mmol) was added to a stirred solution of **6** (17 mg, 0.038 mmol) in 1,4-dioxane (0.50 ml), and the mixture was stirred at 100°C for 1 hour. The mixture was concentrated in vacuo, and the resulting residue was dissolved in MeCN. The solution was purified by preparative HPLC to afford **7** as a purple solid [13.1 mg, 0.0219 mmol as a trifluoroacetic acid (TFA) salt, y. 58%]. ^{1}H NMR ($CDCl_3$, 400 MHz): δ = 7.54 (d, *J* = 9.6 Hz, 1H), 7.45 (d, *J* = 8.7 Hz, 1H), 7.25 (d, *J* = 1.4 Hz, 1H), 7.12 (dd, *J* = 8.7 Hz, 1.4 Hz, 1H), 6.59 (dd, *J* = 9.6 Hz, 2.7 Hz, 1H), 6.25 (d, *J* = 2.7 Hz,1H), 3.65 (m, 2H), 3.21 (s, 3H), 3.09 (t, *J* = 8.2 Hz, 2H), 2.84 (s, 6H), 2.17 (quin, *J* = 8.2 Hz, 2H); ^{13}C NMR ($CDCl_3$, 99 MHz): δ = 158.1, 157.7, 149.5, 135.2, 135.1, 133.4, 125.4, 124.5, 118.1, 115.5, 109.6, 98.9, 54.8, 49.9, 43.0, 39.1, 23.0; ^{11}B NMR ($CDCl_3$, 126 MHz): δ = 0.31; ^{19}F NMR ($CDCl_3$, 369 MHz): δ = −74.6 (3F), −75.1 (3F). Low resolution mass spectrometry (LRMS) [electrospray ionization (ESI)]: *m*/*z* calcd for $[M + H]^+$ 485.1, found 484.9. ESI-HRMS *m*/*z* calcd for $C_{19}H_{22}BBrF_3N_4O_2$ $[M + H]^+$: 485.0960. Found: 485.0966. The position of the introduced amine functionality was confirmed by x-ray crystal structure analysis (fig. S13).

Synthesis of 8

To a solution of **7** (7.9 mg, 0.016 mmol) in *t*BuOH (1.0 ml), HCO_2K (6.8 mg, 0.081 mmol) and $Pd(PPh_3)_4$ (5.7 mg, 0.0049 mmol) were added, and the solution was subjected to freeze-pump-thaw cycles (3×). The mixture was then heated to 90°C for 1 hour. Volatiles were removed under reduced pressure. The resulting residue was dissolved in MeCN and purified by preparative HPLC to afford **8** (1.5 mg as a TFA salt, 0.0029 mmol, y. 18%) as a purple solid. ^{1}H NMR (CD_3CN, 500 MHz): δ = 7.58 to 7.54 (m, 2H), 7.31 (dt, *J* = 8.0 Hz, 1.1 Hz, 1H), 7.03 (m, 2H), 6.78 (dd, *J* = 9.2 Hz, 2.3 Hz, 1H), 6.39 (d, *J* = 2.3 Hz, 1H), 3.66 to 3.59 (m, 2H), 3.20 (s, 3H), 3.07 (m, 2H), 2.76 (s, 6H), 2.06 (m, 2H); ^{13}C NMR ($CDCl_3$, 126 MHz): δ = 158.2, 157.3, 149.3, 135.0, 134.8, 134.2, 132.4, 121.2, 114.9, 114.8, 109.1, 98.9, 55.0, 49.8, 43.1, 39.0, 23.1; ^{11}B NMR ($CDCl_3$, 126 MHz): δ = −0.31; ^{19}F NMR ($CDCl_3$, 369 MHz): δ = −74.4 (3F), −75.2 (3F). LRMS (ESI): *m*/*z* calcd for $[M + H]^+$ 407.2, found 407.0. ESI-HRMS *m*/*z* calcd for $C_{19}H_{23}BF_3N_4O_2$ $[M + H]^+$: 407.1861. Found: 407.1858.

Oxygenation of Aβ and peptide selectivity experiment

The reaction was performed similarly to that described in (*16*). Briefly, stock solutions of $Aβ_{1–42}$ isopeptide (200 μM in 0.1% aqueous TFA), angiotensin-IV (200 μM in water), [Tyr^8]–substance P (200 μM

in water), leuprorelin acetate (200 μM in water), and somatostatin (200 μM in water) were diluted with 0.1 mM phosphate buffer or phosphate-buffered saline (PBS; pH 7.4) to final peptide concentrations of 20 μM (pH 7.4). For $A\beta_{1-42}$, the solution was incubated at 37°C for 3 hours [conditions previously identified for consistent generation of many small fibrils with a high proportion of cross–β-sheet structures (*16*); hereafter, designated as preaggregated $A\beta_{1-42}$]. For preparation of homogeneous oligomer samples, $A\beta_{1-42}$ in phosphate buffer (pH 7.4, 150 mM NaCl included) was incubated for 24 hours at 0°C according to the previous method (*18*). For the control reaction using a less aggregative $A\beta_{1-42}$ isopeptide (*34*), the stock solution above was diluted with Gly-HCl buffer (pH 3.0) to a final peptide concentration of 20 μM.

To each solution, **7** (2 mM in DMSO) was added to a final concentration of 40 μM. The mixture was irradiated with an LED (λ = 595 nm) at 37°C, except for the reaction shown in fig. S3 (at room temperature). Power of the light source for 595-nm LED was 10 mW, and photoirradiation was performed at a distance of approximately 5 cm away from the samples. The temperature increase of the reaction medium during the photooxygenation of $A\beta_{1-42}$ by **7** was less than 1°C in 2 hours. Corresponding reaction samples without light irradiation or **7** were prepared as controls. The reactions were monitored and analyzed using MALDI-TOF-MS. If necessary, an aliquot of the reaction solution was desalted with ZipTip U-C18 (Millipore Corporation) before the MS analysis. The degrees of oxygenation were expressed as the intensity ratio of oxygenation (%) = (sum of MS intensities of n[O] adducts)/(sum of MS peak intensities for remained starting material and n[O] adducts) × 100.

Identification of oxygenation position

To the oxygenation reaction mixture, Glu-C (Sigma-Aldrich, 1:50 of volume) dissolved in water was added, incubated at 37°C for 12 to 16 hours, and analyzed by LC-MS/MS.

Absorbance spectrum of catalysts

5, **6**, or **7** (10 mM in DMSO) was added to $CHCl_3$ or phosphate buffer (final concentration: 20 μM), and the absorbance spectrum was measured.

Absorbance spectrum of 7 in the presence of Aβ

A phosphate-buffered solution (pH 7.4) containing **7** (20 μM) with or without $A\beta_{1-42}$ (20 μM) was incubated at 37°C for 1 hour, and the absorbance spectrum was measured.

Fluorescence spectrum of 7 in the presence of Aβ

The solution for "Absorbance spectrum of **7** in the presence of Aβ" was diluted twice by a phosphate-buffered solution, and the fluorescence spectrum was measured. **7** was excited at 560 nm.

Quartz crystal microbalance

To a gold electrode sensor housed in the cell, 10 μl of 5% EtOH/water including 0.1 mM 20-(11-mercaptoundecanyloxy)-3,6,9,12,15,18-hexaoxaeicosanoic acid was added, the solution was allowed to stand at room temperature for 1 hour, and the sensor was rinsed with water and dried with air blow. Then, to the resulting sensor with self-assembled monolayer on the surface, 50 μl of an aqueous solution including *N*-(3-dimethylaminopropyl)-*N*′-ethylcarbodiimide hydrochloride (50 mg ml^{-1}) and *N*-hydroxy succinimide (50 mg ml^{-1}) was added, the solution was allowed to stand at room temperature for 15 min, and the sensor was rinsed with water and dried with air blow. After the sensor cell was installed into the quartz crystal microbalance apparatus, preaggregated $A\beta_{1-42}$ in phosphate buffer was added to the sensor unit (final volume: 20 μl, 50 μM Aβ, 10 mM phosphate). The solutions were stirred at 25°C until the frequencies become stable. After the sensors were washed with water, 200 μl of 10 mM phosphate buffer (pH 7.4) was added. When a stable baseline was attained, 0.5 μl of DMSO solution containing **7** (0.02, 0.1, 0.5, 2, and 10 mM) was added consecutively, and the changes of the frequencies were measured. The binding curves were generated using KaleidaGraph 4.5. The concentration of **7** that elicited one-half of the maximum change of the frequency was calculated and assigned as K_d value.

Assessment of the production of $^1O_2$

A phosphate buffer solution (pH 7.4) containing the preaggregated $A\beta_{1-42}$ (20 μM), furfuryl alcohol (2 mM), and **7** (0.2 mM) was photoirradiated (595 nm) at 37°C for certain time periods (0, 60, 120, 180, and 240 min), and the concentrations of furfuryl alcohol were quantified by ultraviolet absorbance using HPLC. HPLC method: A linear gradient of 0 to 100% acetonitrile in 0.1% aqueous TFA over 20 min, Triart C18 column, 215 nm.

Calculation

All the calculations were carried out with Gaussian 16 (Revision B.01) program package (*35*). The geometry optimization of ground state and the vibrational analysis of **7**, based on the single-crystal x-ray structure of **10** (fig. S13), were performed by DFT calculation using B3LYP function with SDD basis set for Br atom and 6-311+G(d,p) basis set for all other atoms. The excited-state geometry optimization and the vibrational analysis of **7** were conducted by TD-DFT calculation at the same level of DFT. Furthermore, the relaxed potential energy surface scan for the conformation of dihedral angles at C─N═N─C ($136° < \varphi_{(C-N=N-C)} < 161°$) and the vibrational analysis of **7** in the ground and excited states were performed using DFT and TD-DFT, respectively. ΔG was expressed as relative to the minimum of the ground-state energy.

Oxygenation of amyloids

The reaction was performed similarly to that described in (*16*).

Peptide preparation

Amylin (20 μM in 0.1 M phosphate buffer, pH 7.4) was prepared using an ultracentrifugation in a similar manner as described (*16*). Insulin was dissolved in 25 mM aqueous HCl (400 μM) and stored at −80°C until use. Commercially available solution of α-synuclein [69 μM in 20 mM tris-HCl buffer (pH 7.5), 100 mM NaCl, and 1 mM $MgCl_2$] was stored at −80°C until use.

Amylin

A phosphate buffer solution (pH 7.4) containing amylin (20 μM) was incubated at 37°C for 2 hours, **7** (40 μM) was added thereto, and resulting solution was photoirradiated at 37°C for 2 hours. The reaction mixture was analyzed using MALDI-TOF-MS as above.

Insulin

Neutralized buffer solutions containing insulin [100 μM; "non-aggregated" and "aggregated" samples were prepared via incubation of insulin (400 μM) in 25 mM aqueous HCl solution at 60°C for 0 and 12 hours, respectively] and **7** (40 μM) were photoirradiated at 37°C for 2 hours. The reaction mixture was analyzed using MALDI-TOF-MS.

α-Synuclein

The buffer solution containing α-synuclein (69 μM; aggregated sample was prepared via incubation at 37°C for 24 hours) and **7** (40 μM) was photoirradiated at 37°C for 2 hours. The reaction mixture was treated with Trypsin Gold and analyzed using MALDI-TOF-MS.

ThT assay

The ThT assay was examined in a similar manner as that described in (*16*). Briefly, an aliquot sample (10 μl) of the reaction mixture (20 μM Aβ species, 2 μM **7**, and 0.1 M phosphate) was added to 1.25 μM ThT solution (400 μl), freshly prepared by adding 50 μM ThT in water (10 μl; ThT was purchased from Sigma-Aldrich Inc.) to 50 mM glycine-NaOH buffer (396 μl, pH 8.5). The fluorescence intensity of the solution (400 μl) was measured with 440 nm of an excitation wavelength and 480 nm of an emission wavelength at room temperature. Note that fluorescence intensities of "**7** only" and "**7** + Light" were too low to evaluate the effect of photooxygenation, when 40 μM **7** was applied. Therefore, concentration of **7** was reduced to 2 μM and the reaction time was extended to 18 hours for the ThT assay shown in Fig. 4A. Oxygenation yield for **7** + Light was 28% under these conditions.

Aβ seeding activity

A phosphate buffer (0.1 M, pH 7.4) containing $Aβ_{1–42}$ (20 μM, preaggregated by incubation for 3 hours) and **7** (40 μM) was irradiated at 595 nm for 2 hours. For **7** only sample, the identical mixture was kept in the dark for 2 hours. The photooxygenated or nonoxygenated $Aβ_{1–42}$ was added to $Aβ_{1–40}$ monomer solution (50 μM) with 1 mole percent (mol %) ratio as seed. To evaluate the amount of $Aβ_{1–40}$ fibrils, ThT fluorescence was measured as above. In this experiment, final ThT concentration was 7.5 μM.

Primary neurons

Primary cortical or hippocampal cultures were prepared from brains of E18 Wistar rats as previously described (*12*). Dissociated neurons were plated at 1.0×10^5 cells in 100 μl per well on 96-well plates coated with poly-L-ornithine (Sigma-Aldrich) and cultured in Dulbecco's modified Eagle's medium (DMEM) high glucose (FUJIFILM Wako Pure Chemical Corporation) supplemented with penicillin (50 U/ml), streptomycin (50 μg/ml; Invitrogen), and 10% fetal bovine serum (HyClone). On the following day, the cultured medium was replaced with Neurobasal medium (Invitrogen) supplemented with 2 mM L-glutamine, penicillin (50 U/ml), streptomycin (50 μg/ml), and B-27 supplement (Invitrogen). Cultures were maintained at 37°C under 5% CO_2 until indicated days in vitro (DIV). On the other hand, PBS containing preaggregated $Aβ_{1–42}$ (0 or 20 μM) and **7** (0 or 20 μM) was irradiated with LED (λ = 595 nm) for 1 hour at 37°C. The oxygenated or nonoxygenated Aβ solution (25 μl) was added to the cell plate described above (final Aβ and **7** concentrations were both 5 μM) at DIV7. The cells were incubated for 72 hours at 37°C under 5% CO_2. Cell viability was determined using the Cell Count Reagent SF (Nacalai Tesque Inc., Kyoto, Japan) with WST-8.

PC12 cells

Rat pheochromocytoma PC12 cells suspended in DMEM that contained 5% horse serum and 10% fetal bovine serum were seeded at a density of 10,000 cells per 100 μl per well on a poly-D-lysine–coated 96-well plate and incubated at 37°C under 5% CO_2 for 3 days. After removing the medium, the cells were washed with 150 μl of serum-free DMEM, and 75 μl of DMEM containing 0.1% horse serum was added. Then, the 96-well plate was incubated at 37°C under 5% CO_2 for 1 day. On the other hand, PBS containing preaggregated $Aβ_{1–42}$ (0 or 20 μM) and **7** (0 or 6 μM) was irradiated with LED (λ = 595 nm) for 1 hour at 37°C. The oxygenated or nonoxygenated Aβ solution (25 μl) was added to the cell plate described above (final Aβ and **7** concentration was 5 and 1.5 μM, respectively). The cells were incubated for 48 hours at 37°C under 5% CO_2. Cell viability was determined using the Cell Count Reagent SF (Nacalai Tesque Inc., Kyoto, Japan) with WST-8.

Mouse experiments

All experiments using animals in this study were performed according to the guidelines provided by the Institutional Animal Care Committee of the Graduate School of Pharmaceutical Sciences, The University of Tokyo (protocol no. P31-11). All animals were maintained on a 12-hour light/dark cycle with food and water available ad libitum.

BBB penetration

A solution containing the catalyst (**2**, **3**, or **7**; 1 mM in 10% DMSO/15% Kolliphor EL/75% PBS, 0.2 ml) was intravenously injected into C57BL/6J mice. The mice were perfused with saline, and the brains were excised at 10 min, 60 min, and 24 hours after the injection. The brain samples were homogenized with 1.0 ml MeCN, and the homogenate was centrifuged at 14,000*g* for 5 min at 4°C. The supernatant was collected, and the leftover homogenate was additionally extracted with 1.0 ml MeCN. The combined extracts were filtered and evaporated. The resulting solid was redissolved in 0.1 ml MeCN, and 20 μl of the solution was analyzed by HPLC.

Oxygenation of Aβ in mouse brain lysate

The brain excised from a 7-month-old *App* knock-in ($App^{NL\text{-}G\text{-}F/NL\text{-}G\text{-}F}$) mouse expressing human Arctic Aβs (*29*) was separated into cortex, hippocampus, and remaining brain tissue. The cortex and hippocampus were combined and homogenized in PBS (8 mM $Na_2HPO_4{\cdot}12H_2O$, 2 mM $NaH_2PO_4{\cdot}2H_2O$, 130 mM NaCl), and the suspensions were stored at −80°C until use. **7** was added to the PBS-lysate suspension (final 50 μM) and photoirradiated with LED (λ = 595 nm) or kept in the dark at 37°C. At certain time points, an aliquot of the reaction mixture was diluted with FA (final 70% concentration), evaporated, and redissolved in DMSO. The solution was analyzed on 15% acrylamide/bis mixed solution (29:1) (Nacalai Tesque), with 0.1% SDS running buffer under reducing (1% 2-mercaptoethanol) condition. Molecular weight was estimated with Precision Plus Protein Standards dual color (Bio-Rad, California, USA). Western blotting analysis was performed using anti-Aβ antibody (82E1; IBL).

Oxygenation of off-targets in mouse brain lysate

The cortex and hippocampus from a 7-month-old $App^{NL\text{-}G\text{-}F/NL\text{-}G\text{-}F}$ mouse brain were combined and homogenized using 10× volume of tris buffer [50 mM tris, 150 mM NaCl (pH 7.6), cOmplete EDTA+ (Millipore Sigma, St. Louis, USA)]. Catalyst **7** or riboflavin (50 μM) was added to the lysate, and the mixture was irradiated with 595- or 500-nm light for 2 hours at room temperature. After the reaction, the lysate was centrifuged (260,000*g*, 20 min, 4°C) to obtain a soluble supernatant fraction, and the fraction was analyzed by SDS–polyacrylamide gel electrophoresis (SDS-PAGE) with coomassie brilliant blue (CBB) staining [0.1% CBB R-250 (FUJIFILM Wako Pure Chemical Corporation)/50% MeOH and 10% AcOH].

Fluorescent staining of brain section

The brain of a 6-month-old *App* knock-in ($App^{NL\text{-}G\text{-}F/NL\text{-}G\text{-}F}$) mouse was drop-fixed in 4% paraformaldehyde (FUJIFILM Wako Pure Chemical Corporation) for 24 hours and sliced at 30 μm. For the staining with **7**, the brain sections were incubated with a PBS containing **7** (1 mM) for 15 min and washed with 70% EtOH for 2 min (three times). For the staining with ThS, the brain sections were incubated with a 50% EtOH containing 0.05% ThS (Millipore Sigma, T1892) for 2 min and washed with 70% EtOH for 2 min (three times). The brain sections were mounted on slide glass and imaged using a confocal microscope (TCS-SP5, Leica, Germany) with excitation/emission = 458/490 to 535 nm for ThS and excitation/emission = 543/570 to 650 nm for **7**.

Oxygenation of Aβ in vivo

A solution of **7** (1 mM in 10% DMSO/15% Kolliphor EL/75% PBS, 0.2 ml, ~4.0 mg/kg) was intravenously injected into 11-month-old *App* knock-in ($App^{NL\text{-}G\text{-}F/NL\text{-}G\text{-}F}$) mice expressing human Arctic Aβ. After 60 min, the mice were irradiated with LED (λ = 600 nm) for 10 min. The operation set (catalyst injection and photoirradiation) was repeated five times over 5 days. At 24 hours after the final operation set, the hippocampus was excised. The hippocampus was homogenized using a 10× volume of tris buffered saline (TS) buffer [50 mM tris, 150 mM NaCl (pH 7.6), cOmplete EDTA+ (Roche)]. After the mixture was centrifuged (260,000*g*, 20 min, 4°C), the supernatant was removed, and the precipitate was homogenized using 2% Triton-X–containing TS buffer (equal volume as the TS buffer above). The mixture was then centrifuged (260,000*g*, 20 min, 4°C), and again, the supernatant was removed. The resulting precipitate was homogenized using 70% FA, sonicated, and centrifuged (260,000*g*, 20 min, 4°C). The collected supernatant (=FA fraction) was evaporated, redissolved in DMSO, and analyzed by Western blotting using anti-Aβ antibody (82E1; IBL). The protein subjected to SDS-PAGE was quantified using the bicinchoninic acid method, and the applied amount was normalized.

Quantification of aggregated Aβ in brain after photooxygenation

A solution of **7** (1 mM in 10% DMSO/15% Kolliphor EL/75% PBS, 0.2 ml, ~5.0 mg/kg) was intravenously injected into *App* knock-in ($App^{NL\text{-}G\text{-}F/NL\text{-}G\text{-}F}$) mice (2 to 3 months old) expressing human Arctic Aβs. After 60 min, mice in the **7** + Light mouse group were irradiated with 600-nm LED for 10 min. The operation set (catalyst injection and photoirradiation) was repeated three times per week until the mice were 4 months old (14 to 21 times in total). For the **7** only group, **7** was administered in the same manner, but there was no photoirradiation. At 24 hours after the final operation set, the hippocampus was excised and homogenized using a 10× volume of TS buffer [50 mM tris, 150 mM NaCl (pH 7.6), cOmplete EDTA+ (Roche)]. After the mixture was centrifuged (260,000*g*, 20 min, 4°C), the supernatant was removed, and the precipitate was homogenized using 2% Triton-X–containing TS buffer (equal volume as TS buffer above). The mixture was then centrifuged (260,000*g*, 20 min, 4°C), and again, the supernatant was removed. The resulting precipitate was homogenized using 70% FA, sonicated, and centrifuged (260,000*g*, 20 min, 4°C). The collected supernatant (=FA fraction) was evaporated, redissolved in DMSO, and analyzed by Western blotting using anti-Aβ antibody (82E1; IBL). The protein subjected to SDS-PAGE was quantified using the bicinchoninic acid method, and the applied amount was normalized. The Aβ concentration ratio in **7** + Light is expressed as (Aβ band density in **7** + Light group of mice)/(Aβ band density in **7** only group of mice) × 100.

SUPPLEMENTARY MATERIALS

Supplementary material for this article is available at http://advances.sciencemag.org/cgi/content/full/7/13/eabc9750/DC1

View/request a protocol for this paper from *Bio-protocol*.

REFERENCES AND NOTES

1. A. C. Lai, C. M. Crews, Induced protein degradation: An emerging drug discovery paradigm. *Nat. Rev. Drug Discov.* **16**, 101–114 (2017).
2. C. J. Gerry, S. L. Schreiber, Unifying principles of bifunctional, proximity-inducing small molecules. *Nat. Chem. Biol.* **16**, 369–378 (2020).
3. F. Chiti, C. M. Dobson, Protein misfolding, amyloid formation, and human disease: A summary of progress over the last decade. *Annu. Rev. Biochem.* **86**, 27–68 (2017).
4. M. G. Iadanza, M. P. Jackson, E. W. Hewitt, N. A. Ranson, S. E. Radford, A new era for understanding amyloid structures and disease. *Nat. Rev. Mol. Cell Biol.* **19**, 755–773 (2018).
5. C. Janus, J. Pearson, J. McLaurin, P. M. Mathews, Y. Jiang, S. D. Schmidt, M. A. Chishti, P. Horne, D. Heslin, J. French, H. T. Mount, R. A. Nixon, M. Mercken, C. Bergeron, P. E. Fraser, P. St George-Hyslop, D. Westaway, Aβ peptide immunization reduces behavioural impairment and plaques in a model of Alzheimer's disease. *Nature* **408**, 979–982 (2000).
6. J. Sevigny, P. Chiao, T. Bussière, P. H. Weinreb, L. Williams, M. Maier, R. Dunstan, S. Salloway, T. Chen, Y. Ling, J. O'Gorman, F. Qian, M. Arastu, M. Li, S. Chollate, M. S. Brennan, O. Quntero-Monzon, R. H. Scannevin, H. M. Arnold, T. Engber, K. Rhodes, J. Ferrero, Y. Hang, A. Mikulskis, J. Grimm, C. Hock, R. M. Nitsch, A. Sandrock, The antibody aducanumab reduces Aβ plaques in Alzheimer's disease. *Nature* **537**, 50–56 (2016).
7. C. A. Lemere, Immunotherapy for Alzheimer's disease: Hoops and hurdles. *Mol. Neurodegener.* **8**, 36 (2013).
8. J. Suh, S. H. Yoo, M. G. Kim, K. Jeong, J. Y. Ahn, M.-s. Kim, P. S. Chae, T. Y. Lee, J. Lee, J. Lee, Y. A. Jang, E. H. Ko, Cleavage agents for soluble oligomers of amyloid β peptides. *Angew. Chem. Int. Ed.* **46**, 7064–7067 (2007).
9. J. S. Derrick, J. Lee, S. J. C. Lee, Y. Kim, E. Nam, H. Tak, J. Kang, M. Lee, S. H. Kim, K. Park, J. Cho, M. H. Lim, Mechanistic insights into tunable metal-mediated hydrolysis of amyloid-β peptides. *J. Am. Chem. Soc.* **139**, 2234–2244 (2017).
10. Y. Ishida, S. Tanimoto, D. Takahashi, K. Toshima, Photo-degradation of amyloid β by a designed fullerene–sugar hybrid. *Med. Chem. Commun.* **1**, 212–215 (2010).
11. M. Li, C. Xu, J. Ren, E. Wang, X. Qu, Photodegradation of β-sheet amyloid fibrils associated with Alzheimer's disease by using polyoxometalates as photocatalysts. *Chem. Commun.* **49**, 11394–11396 (2013).
12. A. Taniguchi, D. Sasaki, A. Shiohara, T. Iwatsubo, T. Tomita, Y. Sohma, M. Kanai, Attenuation of the aggregation and neurotoxicity of amyloid-β peptides by catalytic photooxygenation. *Angew. Chem. Int. Ed.* **53**, 1382–1385 (2014).
13. J. S. Lee, B. I. Lee, C. B. Park, Photo-induced inhibition of Alzheimer's β-amyloid aggregation *in vitro* by rose bengal. *Biomaterials* **38**, 43–49 (2015).
14. B. I. Lee, S. Lee, Y. S. Suh, J. S. Lee, A. Kim, O.-Y. Kwon, K. Yu, C. B. Park, Photoexcited porphyrins as a strong suppressor of β-amyloid aggregation and synaptic toxicity. *Angew. Chem. Int. Ed.* **54**, 11472–11476 (2015).
15. B. I. Lee, Y. S. Suh, Y. J. Chung, K. Yu, C. B. Park, Shedding light on Alzheimer's β-amyloidosis: Photosensitized methylene blue inhibits self-assembly of β-amyloid peptides and disintegrates their aggregates. *Sci. Rep.* **7**, 7523 (2017).
16. A. Taniguchi, Y. Shimizu, K. Oisaki, Y. Sohma, M. Kanai, Switchable photooxygenation catalysts that sense higher-order amyloid structures. *Nat. Chem.* **8**, 974–982 (2016).
17. K. N. Solovyov, E. A. Borisevich, Intramolecular heavy-atom effect in the photophysics of organic molecules. *Phys. Usp.* **48**, 231–253 (2005).
18. J. Ni, A. Taniguchi, S. Ozawa, Y. Hori, Y. Kuninobu, T. Saito, T. C. Saido, T. Tomita, Y. Sohma, M. Kanai, Near-infrared photoactivatable oxygenation catalysts of amyloid peptide. *Chem* **4**, 807–820 (2018).
19. T. Suzuki, Y. Hori, T. Sawazaki, Y. Shimizu, Y. Nemoto, A. Taniguchi, S. Ozawa, Y. Sohma, M. Kanai, T. Tomita, Photo-oxygenation inhibits tau amyloid formation. *Chem. Commun.* **55**, 6165–6168 (2019).
20. H. Pajouhesh, G. R. Lenz, Medicinal chemical properties of successful central nervous system drugs. *NeuroRx* **2**, 541–553 (2005).
21. J. Mensch, J. Oyarzabal, C. Mackie, P. Augustijns, In vivo, in vitro and in silico methods for small molecule transfer across the BBB. *J. Pharm. Sci.* **98**, 4429–4468 (2009).
22. M. Gon, K. Tanaka, Y. Chujo, A highly efficient near-infrared-emissive copolymer with a N=N double-bond π-conjugated system based on a fused azobenzene–boron complex. *Angew. Chem. Int. Ed.* **57**, 6546–6551 (2018).

23. J. Mei, N. L. C. Leung, R. T. K. Kwok, J. W. Y. Lam, B. Z. Tang, Aggregation-induced emission: Together we shine, united we soar! *Chem. Rev.* **115**, 11718–11940 (2015).
24. H. F. Kung, C.-W. Lee, Z.-P. Zhuang, M.-P. Kung, C. Hou, K. Plössl, Novel stilbenes as probes for amyloid plaques. *J. Am. Chem. Soc.* **123**, 12740–12741 (2001).
25. W. R. Haag, J. Hoigne, E. Gassman, A. M. Braun, Singlet oxygen in surface waters—Part I: Furfuryl alcohol as a trapping agent. *Chemosphere* **13**, 631–640 (1984).
26. H. LeVine III, Quantification of β-sheet amyloid fibril structures with thioflavin T. *Methods Enzymol.* **309**, 274–284 (1999).
27. K. Hasegawa, I. Yamaguchi, S. Omata, F. Gejyo, H. Naiki, Interaction between Aβ(1−42) and Aβ(1−40) in Alzheimer's β-amyloid fibril formation in vitro. *Biochemistry* **38**, 15514–15521 (1999).
28. H. Fu, M. Cui, L. Zhao, P. Tu, K. Zhou, J. Dai, B. Liu, Highly sensitive near-infrared fluorophores for in vivo detection of amyloid-β plaques in Alzheimer's disease. *J. Med. Chem.* **58**, 6972–6983 (2015).
29. T. Saito, Y. Matsuba, N. Mihira, J. Takano, P. Nilsson, S. Itohara, N. Iwata, T. C. Saido, Single App knock-in mouse models of Alzheimer's disease. *Nat. Neurosci.* **17**, 661–663 (2014).
30. E. F. Marques, M. H. G. Medeiros, P. Di Mascio, Singlet oxygen-induced protein aggregation: Lysozyme crosslink formation and nLC-MS/MS characterization. *J. Mass Spectrom.* **54**, 894–905 (2019).
31. M. Liu, Z. Zhang, J. Cheetham, D. Ren, Z. S. Zhou, Discovery and characterization of a photo-oxidative histidine-histidine cross-link in IgG1 antibody utilizing ^{18}O-labeling and mass spectrometry. *Anal. Chem.* **86**, 4940–4948 (2014).
32. C. F. Xu, Y. Chen, L. Yi, T. Brantley, B. Stanley, Z. Sosic, L. Zang, Discovery and characterization of histidine oxidation initiated cross-links in an IgG1 monoclonal antibody. *Anal. Chem.* **89**, 7915–7923 (2017).
33. G. Leshem, M. Richman, E. Lisniansky, M. Antman-Passig, M. Habashi, A. Gräslund, S. K. T. S. Wärmländer, S. Rahimipour, Photoactive chlorin e6 is a multifunctional modulator of amyloid-β aggregation and toxicity via specific interactions with its histidine residues. *Chem. Sci.* **10**, 208–217 (2019).
34. A. Taniguchi, Y. Sohma, Y. Hirayama, H. Mukai, T. Kimura, Y. Hayashi, K. Matsuzaki, Y. Kiso, "Click peptide": pH-triggered in situ production and aggregation of monomer Aβ1-42. *Chembiochem* **10**, 710–715 (2009).
35. M. J. Frisch, G. W. Trucks, H. B. Schlegel, G. E. Scuseria, M. A. Robb, J. R. Cheeseman, G. Scalmani, V. Barone, G. A. Petersson, H. Nakatsuji, X. Li, M. Caricato, A. V. Marenich, J. Bloino, B. G. Janesko, R. Gomperts, B. Mennucci, H. P. Hratchian, J. V. Ortiz, A. F. Izmaylov, J. L. Sonnenberg, D. Williams-Young, F. Ding, F. Lipparini, F. Egidi, J. Goings, B. Peng, A. Petrone, T. Henderson, D. Ranasinghe, V. G. Zakrzewski, J. Gao, N. Rega, G. Zheng, W. Liang, M. Hada, M. Ehara, K. Toyota, R. Fukuda, J. Hasegawa, M. Ishida, T. Nakajima, Y. Honda, O. Kitao, H. Nakai, T. Vreven, K. Throssell, J. A. Montgomery, Jr., J. E. Peralta, F. Ogliaro, M. J. Bearpark, J. J. Heyd, E. N. Brothers, K. N. Kudin, V. N. Staroverov, T. A. Keith, R. Kobayashi, J. Normand, K. Raghavachari, A. P. Rendell, J. C. Burant, S. S. Iyengar, J. Tomasi, M. Cossi, J. M. Millam, M. Klene, C. Adamo, R. Cammi, J. W. Ochterski, R. L. Martin, K. Morokuma, O. Farkas, J. B. Foresman, D. J. Fox, *Gaussian 16, Revision B.01* (Gaussian Inc., 2016).

Acknowledgments: We appreciate T. C. Saido and T. Saito at Riken Center for Brain Science for providing the AD model mice. The computation was performed at the Research Center for Computational Science, Okazaki, Japan. X-ray single-crystal analysis was conducted at Advanced Characterization Nanotechnology Platform of the University of Tokyo, supported by the "Nanotechnology Platform" of the Ministry of Education, Culture, Sports, Science and Technology (MEXT), Japan. **Funding:** This research was supported by JSPS KAKENHI grant numbers JP16H06216 (Y.S.), JP17H01522 (M.K.), JP20H00489 (M.K.), JP17K19480 (T.T.), JP19H01015 (T.T.), and JP19K22484 (Y.S.) and the Takeda Science Foundation (Y.S.). This research was also supported by the Japanese Agency for Medical Research and Development (AMED) under grant numbers JP19jm0210058 and JP19dm0307030 (Y.S. and Y.H.) and the Brain Mapping by Integrated Neurotechnologies for Disease Studies (Brain/MINDS) (JP18dm0207014 to T.T.). N.N., S.O., and M.O. were supported by a JSPS Research Fellowship for Young Scientists and the Graduate Program for Leaders in Life Innovation (GPLLI). M.F. was supported by a JSPS Research Fellowship for Young Scientists and the World-leading Innovative Graduate Study Program (WINGS). **Author contributions:** N.N., Y.S., and M.K. conceived and designed the research. N.N. and M.F. performed the in vitro experiments. N.N., M.F., and M.O. performed DFT and TD-DFT calculations. N.N. and S.O. performed the in vivo experiments. N.N., S.O., M.F., M.O., Y.H., T.T., Y.S., and M.K. analyzed the data. N.N., Y.S., and M.K. co-wrote the paper. All the authors discussed the results and commented on the manuscript. **Competing interests:** Y.H., T.T., Y.S., and M.K. receive income from Vermilion Therapeutics Inc. for serving as scientific advisory boards. N.N., S.O., Y.H., T.T., Y.S., and M.K. are inventors on a patent application related to this work [no. 2019-217947 (JP), filed on 12 February 2019] and may receive income based on pending license by The University of Tokyo to Vermilion Therapeutics Inc. The authors declare no other competing interests. **Data and materials availability:** All data needed to evaluate the conclusions in the paper are present in the paper and/or the Supplementary Materials. Additional data related to this paper may be requested from the authors.

Submitted 24 May 2020
Accepted 3 February 2021
Published 24 March 2021
10.1126/sciadv.abc9750

Citation: N. Nagashima, S. Ozawa, M. Furuta, M. Oi, Y. Hori, T. Tomita, Y. Sohma, M. Kanai, Catalytic photooxygenation degrades brain Aβ in vivo. *Sci. Adv.* **7**, eabc9750 (2021).

Science Advances

Catalytic photooxygenation degrades brain Aβ in vivo

Nozomu Nagashima, Shuta Ozawa, Masahiro Furuta, Miku Oi, Yukiko Hori, Taisuke Tomita, Youhei Sohma and Motomu Kanai

Sci Adv **7** (13), eabc9750.
DOI: 10.1126/sciadv.abc9750